Measurement of the Flux and Energy Spectrum of Cosmic-Ray Induced Neutrons on the Ground

M. S. Gordon, P. Goldhagen, K. P. Rodbell, T. H. Zabel, H. H. K. Tang, J. M. Clem, and P. Bailey

***Abstract*—New ground-based measurements of the cosmic-ray induced neutron flux and its energy distribution have been made at several locations across the United States using an extended-energy Bonner sphere spectrometer. The data cover over twelve decades of neutron energy, from meV to GeV. An expression to scale the flux to other locations has been developed from a fit to the altitude dependence of our measurements and an expression from the literature for the geomagnetic and solar-activity dependence of neutron monitor rates. In addition, an analytic expression is provided which fits the neutron spectrum above about 0.4 MeV. The neutron flux is important for estimating the soft-error rate in computer memories and recent computer logic devices.**

***Index Terms*—Cosmic rays, neutron flux, neutron radiation effects, neutron spectrometer, neutron spectroscopy, neutron spectrum, neutrons, single event upsets (SEUs), soft errors.**

I. Introduction

WHEN GALACTIC cosmic rays reach the earth's atmosphere, they collide with atomic nuclei in air and create cascades of interactions and reaction products, including neutrons. Some of these neutrons reach the ground. There is ample evidence both experimentally and theoretically that terrestrial neutrons from cosmic rays can be a major source of single event upsets (SEUs) in microelectronics [1]–[6]. Texas Instruments has recently reported that by using a passive alpha-particle mitigation technique, neutrons can be the main source of SEUs [7]. IBM, on the other hand, has recently shown a different trend, where the soft error rate from alpha particles exceeds that due to neutrons from cosmic rays [8]. Unlike alpha particles and heavy ions, neutrons cause SEUs only when they collide with the nucleus of an atom in a device or its packaging, causing the nucleus to recoil or release densely ionizing nuclear fragments. These reaction products cause soft fails when they hit a sensitive area of a semiconductor device. The probability of a neutron producing a nuclear recoil or fragment to which a particular device may be sensitive depends on the neutron's energy [1].

The bit fail cross section characterizes the SEU sensitivity of a circuit. It is determined (e.g., for a memory cell) by loading the memory with a known bit pattern and measuring the number of flipped bits when the device is exposed to a beam of neutrons or charged particles. For particle energy E, the bit fail cross section, $\sigma(E)$, is the measured number of bit flips (or fails) per bit per beam fluence (particles per unit area)

$$\sigma(E) = \frac{\text{fails}}{(\text{bits} \cdot \text{fluence})}. \tag{1}$$

The soft-error failure rate (SER) is then determined by integrating the product of the bit fail cross section and the differential flux over the energy range where the circuit is susceptible to fails

$$\text{SER} = \int \sigma(E) \cdot \left(\frac{d\phi}{dE}\right) dE \tag{2}$$

where $d\phi/dE$ is the fluence rate per unit energy, or differential flux. For neutrons, 10 MeV is often taken to be the lowest energy to which devices are sensitive, but lower-energy neutrons can cause SEUs in certain devices [9], [10], and the impact of neutrons below 10 MeV has become increasingly significant for current technologies due to aggressive scaling of the critical dimensions, reduced voltages, and the use of new materials [11], [12]. Additionally, thermal neutrons have been shown to be an important source for SEUs in devices with borophosphosilicate glass passivation layers containing natural boron, due to the huge thermal-neutron capture cross section of ^{10}B [2], [13].

Accurate measurements of the neutron flux and its energy distribution are important for estimating neutron-induced SER rates. In this paper, data from five ground-level measurements in North America are presented. The neutron flux and energy spectrum were measured using an extended-energy Bonner sphere spectrometer which gave data over more than 12 decades of energy, from meV to GeV [14]–[16]. The intensity of cosmic-ray induced neutrons in the atmosphere varies with altitude, location in the geomagnetic field, and solar magnetic activity [17]–[20]. An expression to scale the measured neutron flux to other locations has been developed from a fit to the altitude dependence of our measurements and an expression from the literature for the geomagnetic and solar-activity dependence of neutron monitor rates. In addition, an analytic expression is provided which fits the portion of the neutron spectrum above about 0.4 MeV.

II. Apparatus and Experimental Method

The extended-energy multisphere (Bonner sphere) neutron spectrometer used for these measurements has been used previously, in a different configuration, for measurements in a high-altitude airplane [14]–[16]. A multisphere spectrometer is a set of moderator spheres surrounding detectors which have high efficiency for detecting thermal-energy neutrons. The larger the moderator, the higher the energy of incident neutrons

Manuscript received July 20, 2004; revised September 16, 2004.

M. S. Gordon, K. P. Rodbell, T. H. Zabel, and H. H. K. Tang are with IBM, T. J. Watson Research Center, Yorktown Heights, NY 10598 USA (e-mail: Gordonm@us.ibm.com).

P. Goldhagen and P. Bailey are with the Environmental Measurements Laboratory, U.S. Department of Homeland Security, New York, NY 10014 USA (e-mail: paul.goldhagn@dhs.gov).

J. M. Clem is with the Bartol Research Institute, University of Delaware, Newark, DE 19716 USA (e-mail: clem@bartol.udel.edu).

Digital Object Identifier 10.1109/TNS.2004.839134

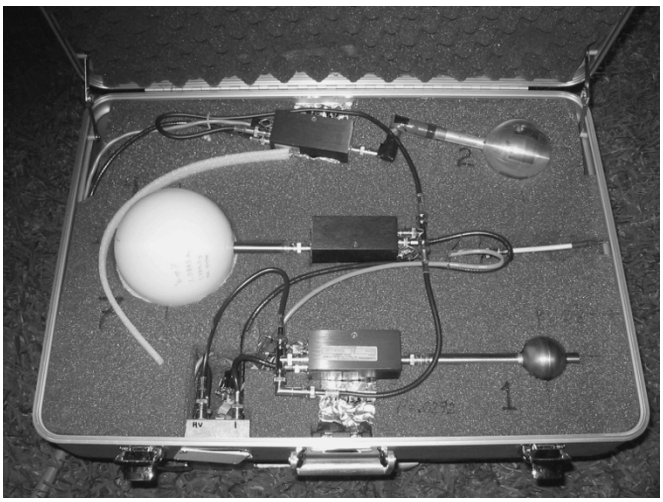

Fig. 1. Three neutron detectors along with their charge-sensitive preamplifiers in a lightweight aluminum suitcase.

Fig. 2. Fourteen-element Bonner sphere spectrometer located on the roof of the IBM T. J. Watson Research Center. The suitcases and connector ends of the large detectors were covered in plastic bags to prevent water damage.

for which the detector assembly has good detection efficiency. If all the detector assemblies are exposed to the same radiation field and the efficiency as a function of energy (response function) of each of the detector assemblies is known, the neutron energy spectrum can be determined from the detector count rates. The 14 detectors of our spectrometer were identical 5.08-cm-diameter spherical ^{3}He-filled proportional counters, with one bare (designated detector 1), one surrounded with a layer of cadmium (detector 2), and the rest surrounded with high-density polyethylene spheres with diameters ranging from 6.7 to 38 cm (detectors 3 to 14). Moderator diameters and masses for all the detectors are given in [16]. To detect neutrons with energies above 30 MeV, detector 13 has a 25-kg lead shell embedded within its 30-cm diameter moderator, and 14 has an 18-kg steel shell in its 38-cm moderator. High-energy neutrons striking the lead or iron nuclei cause hadronic showers with easily detected secondary neutrons, creating a rising response with increasing energy. In addition to detector 2, detectors 4, 6, and 13 were also surrounded by cadmium to reduce their response to thermal neutrons.

Fig. 1 shows a photograph of a group of three detectors as they were deployed in an aluminum suitcase, surrounded by polyurethane foam cushioning. The black boxes are charge-sensitive preamplifiers which were directly attached to each of the proportional counters.

Two other suitcases, containing three detectors each, were part of the spectrometer. The five largest detectors were individually housed in aluminum cylindrical containers—the same containers used for measurements on the airplane. The three suitcases and the five largest detectors were placed on top of lightweight aluminum tables, about 1 m above the ground. When used outdoors, the suitcases and electrical connections were covered with plastic bags to prevent damage from rain, and the tables were tied down to prevent movement due to high winds which occurred at several test sites. At one site (Mt. Washington) the tables were not used and the detector containers were placed on the paved ground. Fig. 2 shows the spectrometer on the roof of the IBM T. J. Watson Research Center in Yorktown Heights, NY.

The data-acquisition electronics and methods were similar to those described in [14]–[16]. After passing through a preamplifier and a purpose-built amplifier, signals from each proportional counter were routed through one of a pair of 8-channel multiplexers to an analog-to-digital converter, and the pulse height stored in a multichannel analyzer in a portable personal computer (PC). Pulse height data were stored on the PC hard drive at intervals commensurate with the counting rate, from once every hour to once every four hours for measurements at high elevation or near sea level, respectively. The large pulses produced by the proton-triton pair from the $^3\mathrm{He}(\mathrm{n},\mathrm{p})^3\mathrm{H}$ neutron capture reaction were cleanly separated from the smaller pulses produced by minimum-ionizing particles and electronic noise. To obtain spectra with high statistical precision, experiments were run until most of the detectors registered well over 10 000 neutron events each, which took over a week at sea level.

Measurements were made outdoors at Fremont Pass, CO; Mount Washington, NH; Yorktown Heights, NY; and Houston, TX. Indoor sites included Leadville, CO, and computer labs at IBM sites in Yorktown Heights, NY, and Burlington, VT. These measurements were made between September 2002 and June 2003. The results from the outdoor sites and the Leadville measurement are presented here. The Leadville measurement could be included with the outdoor measurements because the roof of the one-story building used there was relatively thin ($8.75\ \mathrm{g/cm^2}$), made primarily of wood, and did not significantly change the shape of the measured neutron spectrum. Atmospheric pressure was recorded at each test site so that the neutron measurements could be corrected for the effect of pressure (atmospheric depth).

III. Data Analysis

The response of each detector to neutrons in the energy range 10^{-10} MeV to 100 GeV was calculated using the Monte Carlo radiation transport code MCNPX [21], [22] (versions 2.5.d and 2.5.e). The methods used for calculating these response functions are similar to those used previously [14]–[16]. The effects of the various materials near each detector that were part of the spectrometer were included in the response calculations:

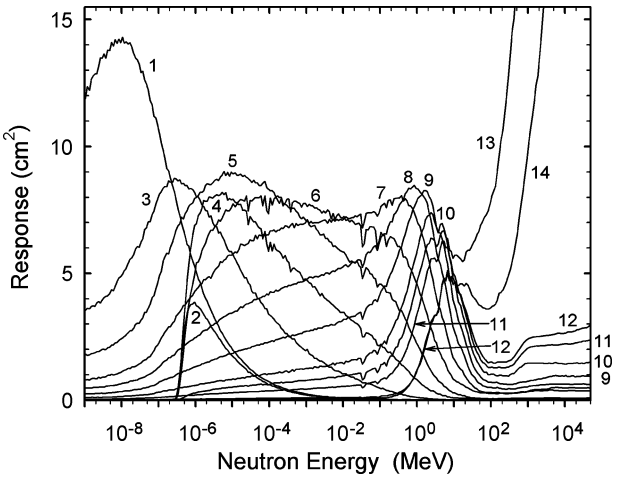

Fig. 3. Calculated neutron response functions for the 14 detectors of the Bonner sphere spectrometer. Response is in counts per $(\mathrm{neutron/cm^2})$, or $\mathrm{cm^2}$. Descriptions of the detectors corresponding to the numbers on each curve are given in Section II and in [16].

each suitcase and its contents was modeled, and the four largest detectors and their containers were modeled together. This accounted for the influence of the two other detectors on the third detector within a suitcase, as well as the influence of the suitcase and padding material. Similarly, the influence of the four largest detectors on each other was calculated. In MCNPX, for energies up to 150 MeV, evaluated neutron cross section data were used. Between 150 MeV and 2 GeV, the CEM2k model [23] of nuclear reactions was used, and for energies above 2 GeV, the Bertini [22], [24] and "scaled Bertini" models [22] were used.

Fig. 3 shows the calculated neutron response functions for each of the detectors. Detector 1, the bare $^3\mathrm{He}$ counter, has a large response to thermal-energy neutrons, and detectors 3 through 12 have responses which peak at increasingly higher energies in accordance with the size of their moderators. Detectors 13 and 14, with their heavy metal converter shells, have very large responses to high-energy neutrons. Detectors 2, 4, 6, and 13 were surrounded by cadmium to limit their response to thermal neutrons. Consequently their response functions show a low-energy cutoff below about $4\times10^{-7}\,\mathrm{MeV}$. The dips in the response functions of all the detectors at energies between about $3\times10^{-2}\,\mathrm{MeV}$ and 0.2 MeV come from nuclear resonances in the aluminum surrounding the detectors, and the response dips for detectors 4 and 6 near $4\times10^{-4}\,\mathrm{MeV}$ come from resonances in cadmium.

Calculated neutron responses for the individual detectors at energies up to about 10 MeV have been verified to within 4% by measurements [25] of a calibrated (NIST-traceable) $^{252}\mathrm{Cf}$ fission neutron source, which has a known energy spectrum. The calibration measurements verified that the geometry and materials were modeled correctly and that the evaluated cross section data we used were selected properly and were accurate. However, the calculations of the responses above 150 MeV use cross sections from nuclear models, which have larger uncertainties, and our high-energy responses have not yet been verified by measurement. We estimate the uncertainty in the response functions above 150 MeV to be 10 to 15%, producing a similar uncertainty in the GeV region of the measured spectra.

Though less numerous than neutrons, protons are also among the secondary cosmic-ray particles in the atmosphere. The spectrometer responds to high-energy protons when they produce neutrons in the metals and carbon in the detectors and their containers. Response functions for protons from 10 MeV to 100 GeV were calculated using MCNPX with the same methods used for neutrons [14]–[16]. Approximate proton count rates were then calculated by folding the proton response functions with secondary cosmic-ray proton spectra calculated by Roesler *et al.* [26], [27]. The calculated proton spectra were scaled to the locations of our measurements using the ratio of our measured neutron flux to the neutron flux that Roesler *et al.* also calculated. The proton count rate was subtracted from the total rate to give the corrected neutron count rate. This correction was always less than 6%.

Once the neutron response function for each of the detectors is known, a deconvolution, or unfolding, computer program is applied to determine the neutron spectrum from the corrected detector count rates. The unfolding code MAXED (version 3.1) was used [28], [29]. In addition to the data and response functions, MAXED requires an initial, or default, spectrum that represents prior knowledge about the shape of the spectrum. From the ensemble of possible spectra that fit the experimental data within its errors, MAXED selects the one which is closest to the default spectrum as measured by the entropy. The program was constrained to use just the shape of the default spectrum and not the amplitude (total fluence rate). While the choice of default spectrum can influence the final measured spectrum, Goldhagen *et al.* have shown that using three different calculated cosmic-ray neutron spectra for the default spectrum gave very similar unfolded measured spectra [16]. Except at thermal energies, calculations by Roesler *et al.* [26], [27] for locations at sea level and 811 $\mathrm{g/cm^2}$ were used as the default spectra for unfolding our measurements. The energy bins of these calculations were also used in the unfolding. The MAXED program applies no smoothing, so any fine structure contained in the default spectrum also shows up in the unfolded spectrum. Broad features in the default spectrum are adjusted to fit the measurement.

IV. Results

A. Neutron Spectrum

Fig. 4 shows the neutron spectrum measured outdoors on a concrete roof in Yorktown Heights, NY. Neutron energy, E, times the fluence rate energy distribution $d\phi/dE$, also called differential flux, is plotted on the vertical axis versus E in MeV with a logarithmic scale on the horizontal axis. The spectrum has three broad peaks: a high-energy peak centered at about 100 MeV and extending up to about 10 GeV, a "nuclear evaporation" peak centered around 1 or 2 MeV, and a thermal peak (neutrons that have been slowed down by scattering until they are in thermal equilibrium with atoms in surrounding materials). Between the evaporation peak and the thermal peak, there is a plateau region where $d\phi/dE$ is approximately proportional to $1/E$. The evaporation peak has fine structure from nuclear resonances in the nitrogen and oxygen of the atmosphere and in materials in the concrete roof. Most of this structure is finer than

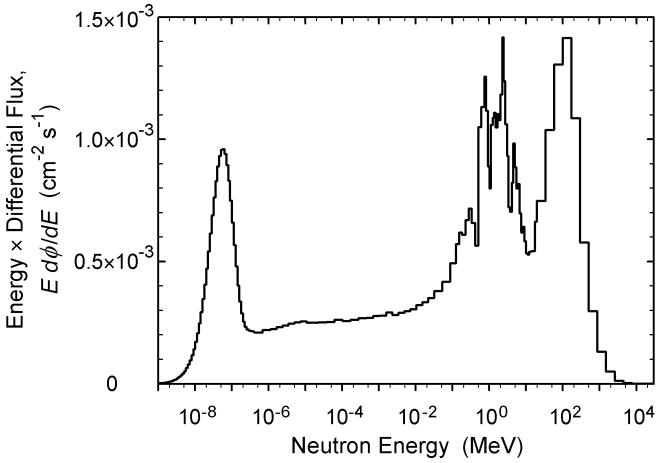

Fig. 4. Neutron spectrum measured on the roof of the IBM T. J. Watson Research Center in Yorktown Heights, NY.

the resolution of the spectrometer, and it appears in the measured spectrum because it is present in the calculated spectrum [26], [27] used as the default spectrum for the unfolding.

The representation of the neutron spectrum in Fig. 4 is standard in the field of radiation protection, but not in the literature on SEUs or cosmic-ray physics. It is conceptually simpler to plot $d\phi/dE$, but for neutrons, that typically requires a log-log plot covering many orders of magnitude on both axes, making details difficult to see. The large range of neutron $d\phi/dE$ stems from its characteristic $1/E$ dependence when neutrons slow down in a scattering medium. $E(d\phi/dE)$ is relatively flat and can be plotted on a linear scale. $E(d\phi/dE)$ is mathematically identical to $d\phi/d(\ln(E))$. In a plot of $E(d\phi/dE)$ against $\log(E)$, equal areas under the spectrum in different energy regions represent equal integral fluxes. In Fig. 4, it is visually apparent that about 30% of the neutron flux in the measured spectrum is at energies above 10 MeV.

The total neutron flux at this location was 0.0134 $\mathrm{cm^{-2}\ s^{-1}}$, which is 6% higher than an earlier measurement by Goldhagen *et al.* at sea level in Hampton, VA, and about 250 times lower than the flux measured on an airplane at 12 km altitude over Oakland, CA [14].

B. Trends in the Neutron Flux

The intensity of cosmic-ray induced neutrons (and other secondary cosmic radiation) in the atmosphere varies with altitude, location in the geomagnetic field, and solar magnetic activity [17]–[20]. Atmospheric shielding at a given altitude is determined by the mass thickness per unit area of the air above, called atmospheric depth. The geomagnetic field deflects low-momentum primary cosmic particles back into space, lowering the neutron flux produced in the atmosphere. The minimum momentum per unit charge (magnetic rigidity) that an incident (often, vertically incident) particle can have and still reach a given location above the earth is called the geomagnetic cutoff rigidity (cutoff) for that point. The varying magnetic field carried outward from the sun by the solar wind plasma that permeates the solar system also reduces the cosmic-ray intensity at earth. This solar modulation has been measured for decades by a number of neutron monitors on the ground at various locations, [30]–[32] for example. The cosmic-ray induced neutron flux is highest when solar activity is at a minimum (solar minimum), and lowest during solar maximum.

As will be shown below, the *shape* of the outdoor ground-level neutron spectrum above ~5 MeV does not change significantly with altitude, cutoff, or solar modulation. To account for the effects of these variables on the total flux, the neutron fluence rate spectrum outdoors at any location can be expressed as follows:

$$\frac{d\phi(E)}{dE} = \frac{d\phi_0(E)}{dE} \cdot F_{\mathrm{alt}}(d) \cdot F_{\mathrm{BSYD}}(R_{\mathrm{c}}, d, I) \qquad (3)$$

where $d\phi_0(E)/dE$ is the fluence rate spectrum at a reference location (e.g., New York City at sea level and mid-value solar modulation), d is the atmospheric depth, R_c is the vertical geomagnetic cutoff rigidity, I is the relative count rate of a neutron monitor measuring solar modulation, $F_{alt}(d)$ is a function describing the dependence on altitude (i.e., on atmospheric depth) and $F_{\mathrm{BSYD}}(R_{\mathrm{c}}, d, I)$ is a function describing the dependence on geomagnetic location and solar modulation (and also depth). Atmospheric depth is given by $d = h/g$, where h is the barometric pressure and g is the acceleration of gravity. Vertical cutoff depends primarily on the horizontal component of the earth's magnetic field. It is near zero at the poles and has a maximum of 15 to 17 GV at the equator. (GV is a unit of rigidity, GeV is a unit of energy.) Consequently, the cosmic-ray induced neutron flux is higher at the poles and lower at the equator. Values of R_c for cosmic rays reaching the atmosphere have been calculated by Shea and Smart [33] for a grid of locations covering the globe and updated for the Federal Aviation Administration [34].

In (3), the main altitude dependence is exponential attenuation

$$F_{\mathrm{alt}}(d) = \exp\left[\frac{(d_{\mathrm{SL}} - d)}{L_{\mathrm{n}}}\right] \qquad (4)$$

where $d_{SL} = 1033.7\ \mathrm{g/cm^2}$ is the atmospheric depth at sea level, and $L_n = 131.3\ \mathrm{g/cm^2}$ is the effective attenuation length in the atmosphere for neutrons above 10 MeV, as determined by the fit to the data described below. F_{alt} varied by almost a factor of 15 from sea level to the 3450 m altitude of the measurement site at Climax, CO,—a far larger variation than the global variation with cutoff, which is about a factor of 2 from equator to pole at sea level, and 3 at the highest inhabited altitudes. Solar modulation is smaller still, about a 25% decrease from maximum to minimum recorded monthly-averaged rates at polar locations near sea level (McMurdo and Oulu neutron monitors [30], [31]) and ~7% at the equator, and 30% to 12% for polar and equatorial sites at high elevations (Climax and Huancayo-Haleakala monitors [32]).

The function $F_{\mathrm{BSYD}}(R_{\mathrm{c}}, d, I)$ in (3) is a depth-dependent Dorman function developed by Dorman and Yanke and parameterized by Belov, Struminsky, and Yanke (BSY) to describe the location dependence of ground neutron monitor rates in terms of cutoff and barometric pressure [35], [36]. It has the general form

$$F_{\mathrm{BSYD}}(R_{\mathrm{c}}, d, I) = N\left[1 - \exp\left(\frac{-\alpha}{R_c^k}\right)\right] \qquad (5)$$

TABLE I
DATA RELATING TO THE MEASUREMENT LOCATIONS

Site	Alt. (m)	Atmosph. depth (g/cm^2)	R_c (GV)	F_{BSYD} (11/02)	Solar modulation factor	F_{alt}
Fremont Pass, CO	3450	682.6	2.94	0.874	1.005	14.74
Leadville, CO	3150	719.7[a]	2.97	0.880	1.010	11.09
Mt. Wash. NH	1905	826.6	1.58	0.970	0.990	4.89
Yorktown Hts., NY	167	1011.3	2.00	0.997	1.000	1.19
Houston, TX	14	1028.0	4.68	0.896	1.008	1.04

[a] Includes 8.75 g/cm^2 for the roof in Leadville

where N is a normalization factor, and α and k depend on pressure (depth) and solar modulation. Values of these parameters for solar minimum and maximum (S_{min} and S_{max}) were derived by BSY, and are given in the Appendix, along with a table of values of $F_{BSYD}(R_c)$ for sea level and mid-value solar modulation, normalized so $F_{BSYD}(R_{c,NYC}) = 1$. F_{BSYD} fits the observed cutoff dependence and monthly-averaged solar modulation of the rates of many neutron monitors reasonably well for all the observed solar cycles except for the extremely low rates between 1989 and 1991.

To compare our measurements at the different locations, fit (4) to them, and determine the best value for L_n, we used the flux integrated above 10 MeV, because neutrons at lower energies come partly from scatter in local materials which varied from site to site. The measured high-energy flux was divided by F_{BSYD} at the cutoff and depth of each location. Our measurement with the most data, the one at Yorktown Heights, was done at a time (November 2002) when neutron monitor count rates were about 20% of the way from their typical minimum values, at S_{max}, to their maximum values, at S_{min}. Since we have parameters from BSY only for S_{max} and S_{min}, we obtained F_{BSYD} for the time of the measurement by interpolating 20% of the way from $F_{BSYD,Smax}$ to $F_{BSYD,Smin}$.

Since the data from the 5 measurements presented here spanned a period of about 9 months, there was a slight change in the flux between measurements due to changes in solar modulation. To compensate, the ratio of a neutron monitor count rate at the time of each measurement relative to the time of the Yorktown Heights measurement, I/I_0, was used as a measure of solar modulation, and this ratio was multiplied by F_{BSYD} for the cutoff and depth of each measurement location to obtain a solar modulation factor. This correction was 1% or less. Any neutron monitor could be used; we used data from the one in Newark, Delaware [30].

Table I shows data relating to each of the measurement locations, including altitude, atmospheric depth, cutoff, $F_{BSYD}(R_c, d)$ for November 2002, the solar modulation factor, and the value of $F_{alt}(d)$ resulting from a fit of (4) to the corrected high-energy fluxes. The high energy flux data were corrected by dividing by F_{BSYD} and the solar modulation factor. The corrected data and the fit are shown in Fig. 5.

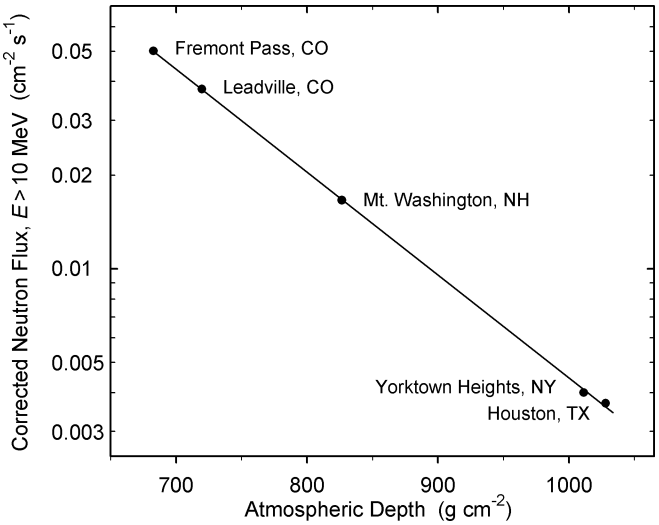

Fig. 5. Neutron flux above 10 MeV at 5 measurement locations as a function of atmospheric depth (points). The data have been corrected for location-dependent geomagnetic cutoff and variations in solar modulation as described in the text and fit with (4) (line).

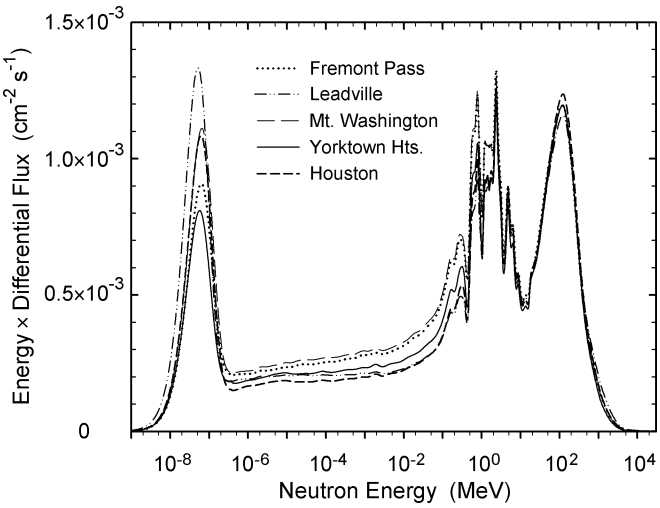

Fig. 6. Measured neutron spectra for all five sites. Each spectrum has been scaled to sea level at the cutoff of New York City and solar modulation for November 2002, as described in the text.

From the least-squares fit shown in Fig. 5, the neutron attenuation length was determined to be 131.3 ± 1.3 g/cm^2. The largest fit residual $((\text{fit} - \text{data})/\text{data})$ occurred for the two data points near sea level (Yorktown Heights and Houston) and amounted to $\pm 2.35\%$. If the measured flux had not been corrected for F_{BSYD}, the fitted attenuation length would have been 135.0 g/cm^2 and the fit to the data would not have been as good, with residuals of up to $+4.2\%$ and -4.9%.

To compare the shapes of the measured spectra at the 5 locations, the spectra were scaled by applying the same corrections used for the fit shown in Fig. 5 and then divided by $F_{alt}(d)$ for each location (the last column of Table I). The resulting spectra are shown in Fig. 6. Above a few MeV, the spectra practically lie on top of one another, justifying the assumption in (3) that one spectral shape can be used at various locations, at least for the limited range of cutoffs covered by our measurements

TABLE II
FITTED PARAMETERS FOR THE ANALYTIC MODEL

j	β_j	γ_j	c_j
1	0.3500	2.1451	1.006×10^{-6}
2	0.4106	-0.6670	1.011×10^{-3}

($R_c < 5$ GV). In the Appendix, we provide a table of numerical values of neutron differential flux, $d\phi_0/dE$, for $E \geq 1$ MeV determined from the shape of the Yorktown Heights spectrum scaled down to the location of New York City (NYC) at sea level (as it is shown in Fig. 6), then further adjusted up to the fit in Fig. 5, and up to the mid-point of solar modulation using (3). We refer to this spectrum as the "reference" spectrum. Its flux is 0.901 times that of the measured spectrum at Yorktown Heights and 1.07 times that of the scaled spectrum shown in Fig. 6.

The spectrum may change shape slightly in the GeV region at higher cutoffs. The airplane measurements of Goldhagen *et al.* [14], obtained at an altitude of 20 km, found that the fraction of the total flux that was above 10 MeV was 8% higher at a cutoff of 11.8 GV than at 0.8 GV. Calculations by Mares *et al.* [37] show that the cutoff dependence of the spectrum shape is less than half as much on the ground as it is at 20 km.

V. ANALYTIC MODEL

In addition to tabulated values of $d\phi_0/dE$, a simple analytic expression has been fit to the NYC reference neutron spectrum in the energy range from 0.1 MeV to 10 GeV

$$\frac{d\phi_0(E)}{dE} = \sum_{j=1}^{2} c_j \exp\left[-\beta_j \left(\ln(E)\right)^2 + \gamma_j \ln(E)\right]. \quad (6)$$

The values of the parameters c_j, β_j, and γ_j in (6) were constrained by requiring that the energy-integrated fluence, $\int(d\phi/dE)dE$, in the energy regions of the evaporation and high-energy peaks from the model agree with the experimental data to within a few percent. The numerical values of these parameters are listed in Table II. Since the flux in the thermal peak, and to a lesser extent the plateau region, depend on the local environment, functions fitting these regions are not presented here.

Fig. 7 shows a graph of the evaporation and high-energy regions of the reference spectrum and the analytic model in the $E(d\phi/dE)$ representation. The data are shown as a histogram and the analytic model is the solid smooth curve. The fit is visibly very good above 10 MeV and reasonably good in the evaporation region down to about 0.4 MeV.

VI. COMPARISON TO JEDEC STANDARD

Fig. 7 also shows the spectrum from Appendix E of JEDEC Standard JESD89 [38]. The JEDEC model was a fit through previously published data adjusted to the same conditions as our reference spectrum. (This was the main reason we chose those conditions.) It has been used for a number of years and forms the basis of current SER calculations. The JEDEC model underestimates the reference measured flux integrated from 50 MeV to 1 GeV ($\mathrm{JEDEC/measured} = 0.75$) and overestimates

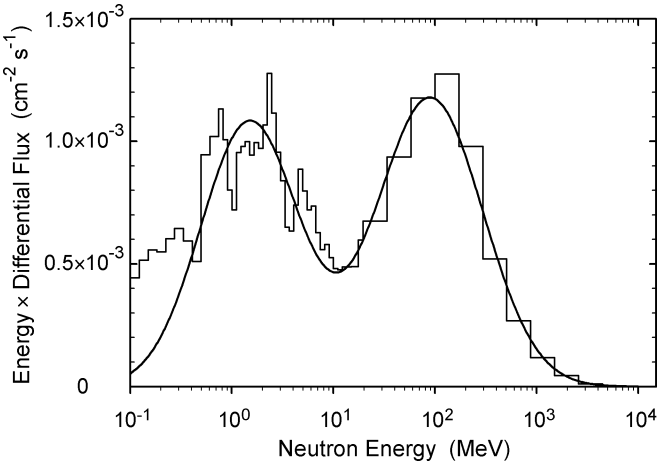

Fig. 7. Upper-energy portion of the reference neutron spectrum at New York City, sea level, and mid-level solar modulation (histogram), the analytic fit (solid smooth curve), and the model from Appendix E of JEDEC Standard no. 89 [38] (dashed curve).

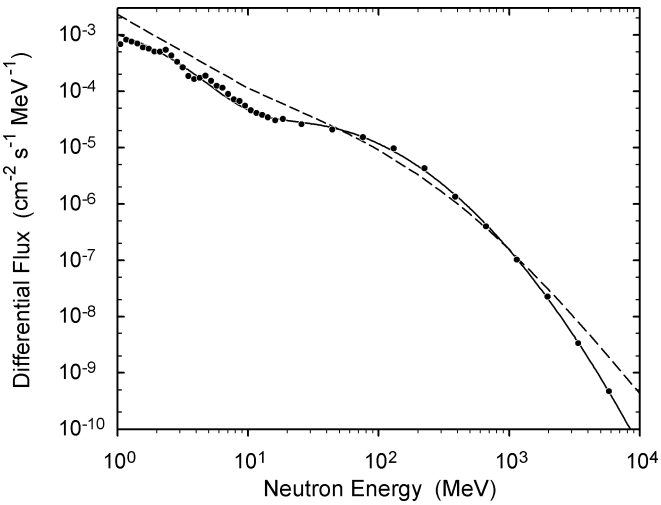

Fig. 8. Differential flux, $d\phi/dE$, ($\mathrm{cm^{-2}\ s^{-1}\ MeV^{-1}}$) of cosmic-ray induced neutrons as a function of neutron energy. The data points are our reference spectrum from the measurements, the solid curve is our analytic model, and the dashed curve is the JEDEC model [38].

it from 5 to 50 MeV and again from 1 to 10 GeV by factors of 1.7 and 1.3, respectively.

Fig. 8 shows the same data as Fig. 7, but presented as the more familiar differential flux (neutrons $\mathrm{cm^{-2}\ s^{-1}\ MeV^{-1}}$). As already shown in Fig. 7, our analytic model reproduces the measured spectrum better than the JEDEC model.

VII. CONCLUSION

Five sets of neutron spectrometer data have been collected and analyzed from a variety of sites across the United States to determine the flux and energy distribution of cosmic-ray induced neutrons on the ground. The measurement sites had a wide range of altitudes and a small range of geomagnetic cutoff rigidities (1.6 to 4.7 GV). An extended-energy Bonner sphere spectrometer was used that collected data simultaneously across an energy range from 1 meV to about 10 GeV. The measured total neutron flux varied by a factor of 15 from the highest to lowest altitude sites, but the shape of the spectrum above

10 MeV was almost independent of altitude and geomagnetic cutoff rigidity. The dominant uncertainty in the high-energy region of the measured spectra comes from the 10 to 15% uncertainty in the spectrometer detector response functions above 150 MeV. Analysis of trends at high altitude shows that the additional error in the ground-level flux above 10 MeV at high cutoffs that might be caused by assuming a constant spectral shape is less than 4%.

Values of the neutron differential flux for reference conditions (New York City, sea level, mid-level solar modulation) are given in a table. In addition, an analytic expression is provided which fits the portion of the neutron spectrum above about 0.4 MeV. An expression to scale the measured neutron flux to other locations has been developed from an exponential attenuation fit to the altitude dependence of our measurements and an expression from the literature for the geomagnetic and solar-activity dependence of neutron monitor rates. A table of values for the cutoff dependence at sea level and average solar modulation is also provided.

APPENDIX

Here we give the values for the parameters in (5), the scaling function for geomagnetic cutoff, determined by Belov, Struminsky, and Yanke (BSY) at solar minimum and maximum, $F_{\mathrm{BSYD,Smin}}$ and $F_{\mathrm{BSYD,Smax}}$ [35], [36], normalized so that their mean, $F_{\mathrm{BSYD,Smid}}$, is 1 at NYC at standard sea-level pressure. We also give a table of values of $F_{\mathrm{BSYD,Smid}}(R_c)$ at sea level, and then a table of values of $d\phi/dE$ for our reference spectrum.

BSY used barometric pressure, h, in bar ($1\ \mathrm{bar} = 10^5\ \mathrm{Pa}$) instead of depth. With depth, d, in $\mathrm{g/cm^2}$, $h = 9.8025 \times 10^{-4} d$. The renormalized BSYD functions for $\mathrm{S_{min}}$ and $\mathrm{S_{max}}$ are

$$F_{\mathrm{BSYD,Smin}}(Rc, h) = 1.098\left[1 - \exp\left(\frac{-\alpha_1}{R_c^{k_1}}\right)\right] \quad \text{(A-1)}$$

and

$$F_{\mathrm{BSYD,Smax}}(R_c, h) = 1.098\left[1 - \exp\left(\frac{-\alpha_2}{R_c^{k_2}}\right)\right] \times \left[1 - \exp\left(-\alpha_1/50^{k_1}\right)\right] / \left[1 - \exp\left(-\alpha_2/50^{k_2}\right)\right] \quad \text{(A-2)}$$

where the parameters α and k are given by

$$\alpha_1 = \exp\left[1.84 + 0.094h - 0.09\exp(-1.1h)\right] \quad \text{(A-3)}$$

$$k_1 = 1.4 - 0.56h + 0.24\exp(-8.8h) \quad \text{(A-4)}$$

$$\alpha_2 = \exp\left[1.93 + 0.15h - 0.18\exp(-10h)\right] \quad \text{(A-5)}$$

$$\text{and}\ \ k_2 = 1.32 - 0.49h + 0.18\exp(-9.5h). \quad \text{(A-6)}$$

(A-1) and (A-2) are normalized so their mean is 1 at New York City at standard sea-level pressure, $h = 1.013\,25$ bar. We have not attempted to derive values for the parameters at other solar modulations; we simply interpolate between (A-1) and (A-2).

Values for $F_{\mathrm{BYSD,Smid}}(R_c)$, the mean of (A-1) and (A-2), at sea level for the global range of R_c are given in Table A-I.

Values of the differential flux for the upper-energy portion of the reference neutron spectrum at NYC, sea level, and mid-level solar modulation (scaled from the rooftop Yorktown Heights measurement) are given in Table A-II as a function of energy. The differential flux for a location at a given cutoff and depth may be obtained by multiplying this reference spectrum by an interpolated value between $F_{\mathrm{BYSD,Smin}}$ and $F_{\mathrm{BYSD,Smax}}$ (or just their average, which will generally be accurate to $\pm 10\%$) and by F_{alt} from (4).

TABLE A-I
VALUES OF THE SCALING FUNCTION $F_{\mathrm{BSYD,Smid}}(R_c)$ AT SEA LEVEL

Vertical Cutoff (GV)	$F_{\mathrm{BYSD,\ Smid}}$	Vertical Cutoff (GV)	$F_{\mathrm{BYSD,\ Smid}}$
0	1.019	9	0.712
1	1.018	10	0.679
2	1.002	11	0.650
3	0.966	12	0.623
4	0.920	13	0.598
5	0.873	14	0.576
6	0.828	15	0.555
7	0.786	16	0.536
8	0.747	17	0.518

TABLE A-II
VALUES OF THE NEUTRON DIFFERENTIAL FLUX FOR REFERENCE CONDITIONS (NYC, SEA LEVEL, MID-LEVEL SOLAR MODULATION)

Energy (MeV)	$d\phi_0/dE$ ($\mathrm{cm^{-2}s^{-1}MeV^{-1}}$)	Energy (MeV)	$d\phi_0/dE$ ($\mathrm{cm^{-2}s^{-1}MeV^{-1}}$)
1.054	6.83×10^{-4}	10.51	4.58×10^{-5}
1.165	8.19×10^{-4}	11.62	4.09×10^{-5}
1.287	7.61×10^{-4}	12.84	3.80×10^{-5}
1.423	7.02×10^{-4}	14.19	3.44×10^{-5}
1.572	6.00×10^{-4}	16.16	3.02×10^{-5}
1.738	5.72×10^{-4}	18.52	3.22×10^{-5}
1.920	5.06×10^{-4}	25.70	2.59×10^{-5}
2.122	5.02×10^{-4}	44.19	2.09×10^{-5}
2.346	5.44×10^{-4}	75.98	1.53×10^{-5}
2.592	4.30×10^{-4}	130.7	9.64×10^{-6}
2.865	3.34×10^{-4}	224.6	4.30×10^{-6}
3.166	2.65×10^{-4}	386.3	1.33×10^{-6}
3.499	1.86×10^{-4}	664.2	3.99×10^{-7}
3.867	1.64×10^{-4}	1.142×10^{3}	1.02×10^{-7}
4.274	1.73×10^{-4}	1.964×10^{3}	2.24×10^{-8}
4.724	1.88×10^{-4}	3.376×10^{3}	3.36×10^{-9}
5.220	1.53×10^{-4}	5.805×10^{3}	4.71×10^{-10}
5.769	1.25×10^{-4}	9.982×10^{3}	9.87×10^{-11}
6.376	1.16×10^{-4}	1.716×10^{4}	3.83×10^{-11}
7.047	8.90×10^{-5}	2.951×10^{4}	8.60×10^{-12}
7.788	7.16×10^{-5}	5.074×10^{4}	2.17×10^{-12}
8.607	6.73×10^{-5}	8.725×10^{4}	6.97×10^{-13}
9.512	5.53×10^{-5}	1.500×10^{5}	1.88×10^{-13}

ACKNOWLEDGMENT

The authors would like to acknowledge the help of their colleagues, including M. Talus, who allowed them us to use his lawn for the Houston measurements, and K. Rancourt for arranging the use of the facilities at the Mt. Washington Observatory. They would also like to thank the SER group at IBM, including D. Heidel, E. Cannon, T. Ning, K. Bernstein, P. Oldiges, and D. Rheinhardt. Neutron Monitores of the Bartol Research Institute were supported by the National Science Foundation under Grant ATM-0000315.

REFERENCES

[1] H. H. K. Tang and K. P. Rodbell, "Single-event upsets in microelectronics," *MRS Bulletin*, vol. 28, no. 2, pp. 111–116, Feb. 2003.

[2] R. Baumann, "Impact of single-event upsets in deep-submicron silicon technology," *MRS Bulletin*, vol. 28, no. 2, pp. 117–120, Feb. 2003.

[3] T. J. O'Gorman *et al.*, "Field testing for cosmic ray soft errors in semiconductor memories," *IBM J. Res. Develop.*, vol. 40, no. 1, pp. 41–50, Jan. 1996.

[4] G. R. Srinivasan, "Modeling the cosmic-ray-induced soft-error rate in integrated circuits: an overview," *IBM J. Res. Develop.*, vol. 40, no. 1, pp. 77–89, Jan. 1996.

[5] P. C. Murley and G. R. Srinivasan, "Soft-error Monte Carlo modeling program, SEMM," *IBM J. Res. Develop.*, vol. 40, no. 1, pp. 109–118, Jan. 1996.

[6] H. H. K. Tang, "Nuclear physics of cosmic ray interaction with semiconductor materials: particle-induced soft-errors from a physicist's perspective," *IBM J. Res. Develop.*, vol. 40, no. 1, pp. 91–108, Jan. 1996.

[7] R. Baumann, private communication, June 2004.

[8] E. H. Cannon, D. D. Reinhardt, M. S. Gordon, and P. S. Makowenskij, "SRAM SER in 90, 130 and 180 nm bulk and SOI technologies," in *Proc. 2004 IEEE Int. Reliability Physics Symp.*, Aug. 2004, pp. 300–304.

[9] E. Normand, J. L. Wert, W. R. Doherty, D. L. Oberg, P. R. Measel, and T. L. Criswell, "Use of PuBe source to simulate neutron-induced single event upsets in static RAMs," *IEEE Trans. Nucl. Sci.*, vol. 35, pp. 1523–1528, Dec. 1988.

[10] D. Thouvenot, P. Trochet, R. Gaillard, and F. Desnoyers, "Neutron single effect test results for various memories," in *Proc. 1997 IEEE Radiation Effects Data Workshop*, July 1997, pp. 61–66.

[11] Y. Yahagi *et al.*, "Threshold energy of neutron-induced single event upsets as a critical factor," in *Proc. 2004 IEEE Int. Reliability Physics Symp.*, Aug. 2004, pp. 669–670.

[12] K. Johansson *et al.*, "Energy-resolved neutron SEU measurements from 22 to 160 MeV," *IEEE Trans. Nucl. Sci.*, vol. 45, pp. 2519–2526, Dec. 1998.

[13] R. Fleischer, "Cosmic ray interactions with boron: a possible source of soft errors," *IEEE Trans. Nucl. Sci.*, vol. NS-30, pp. 4013–4015, Oct. 1983.

[14] P. Goldhagen, J. M. Clem, and J. W. Wilson, "The energy spectrum of cosmic-ray induced neutrons measured on an airplane over a wide range of altitude and latitude," *Radiat. Prot. Dosim.*, vol. 110, no. 1–4, pp. 387–392, Sep. 2004.

[15] ——, "Recent results from measurements of the energy spectrum of cosmic-ray induced neutrons aboard an ER-2 airplane and on the ground," *Adv. Space Res.*, vol. 32, no. 1, pp. 35–40, July 2003.

[16] P. Goldhagen, M. Reginatto, T. Kniss, and J. W. Wilson *et al.*, "Measurement of the energy spectrum of cosmic-ray induced neutrons aboard an ER-2 high-altitude airplane," *Nucl. Instrum. Meth. A*, vol. 476, no. 1–2, pp. 42–51, Jan. 2002.

[17] P. Goldhagen, "Cosmic-ray neutrons on the ground and in the atmosphere," *MRS Bulletin*, vol. 28, no. 2, pp. 131–135, Feb. 2003.

[18] W. Heinrich, S. Roesler, and H. Schraube, "Physics of cosmic radiation fields," *Radiat. Prot. Dosim.*, vol. 86, no. 4, pp. 253–258, 1999.

[19] J. F. Ziegler, "Terrestrial cosmic ray intensities," *IBM J. Res. Develop.*, vol. 42, no. 1, pp. 117–140, Jan. 1998.

[20] E. Normand and T. J. Baker, "Altitude and latitude variation in avionics SEU and atmospheric neutron flux," *IEEE Trans. Nucl. Sci.*, vol. 40, p. 1489, Dec. 1993.

[21] H. G. Hughes, R. E. Prael, and R. C. Little, "MCNPX—the LAHET/MCNP code merger,", Los Alamos, NM, Los Alamos National Lab. Rep. XTM-RN(U)97-012, 1977.

[22] *MCNPX User's Manual, Version 2.3.0*, L. S. Waters, Ed., Los Alamos Nat. Lab., Los Alamos, NM, 2002.

[23] S. G. Mashnik and A. J. Sierk, "Recent developments of the cascade-exciton model of nuclear reactions," in *Proc. ND'01 Journal Nuclear Science Technology*, Tsukuba, Japan, 2002, pp. 720–725.

[24] H. W. Bertini, "Intranuclear-cascade calculation of the secondary nucleon spectra from nucleon-nucleus interactions in the energy range 340 to 2900 Mev and comparisons with experiment," *Phys. Rev.*, vol. 188, no. 4, pp. 1711–1730, Dec. 1969.

[25] T. A. Kniss, "Monte Carlo calculation of the response of a multisphere neutron spectrometer and comparison with experimental measurements," M.Sc. thesis, Univ. Akron, Akron, OH, 1996.

[26] S. Roesler, W. Heinrich, and H. Schraube, "Monte Carlo calculation of the radiation field at aircraft altitudes," *Radiat. Prot. Dosim.*, vol. 98, no. 4, pp. 367–388, 2002.

[27] S. Roesler, private communication, 2001.

[28] M. Reginatto and P. Goldhagen, "MAXED, a computer code for the deconvolution of multisphere neutron spectrometer data using the maximum entropy method," U.S. Dept. Energy Environmental Measurements Lab., New York, Tech. Rep. EML-595, June 1998.

[29] ——, "MAXED, a computer code for maximum entropy deconvolution of multisphere neutron spectrometer data," *Health Phys.*, vol. 77, no. 5, pp. 579–583, 1999.

[30] J. W. Bieber *et al.*. University of Delaware Bartol Research Institute Neutron Monitor Program. [Online]. Available: http://www.bartol.udel.edu/~neutronm/

[31] I. Usoskin. Oulu Cosmic Ray Station. [Online]. Available: http://cosmicrays.oulu.fi/

[32] C. Lopate. Climax and Haleakala Neutron Monitor Datasets. [Online]. Available: http://ulysses.sr.unh.edu/NeutronMonitor/neutron_mon.html

[33] M. E. Shea and D. F. Smart, "Tables of asymptotic directions and vertical cutoff rigidities for a five degree by fifteen degree world grid as calculated using the international geomagnetic reference field for epoch 1975.0," Air Force Geophysics Laboratory, Hanscom AFB, Massachusetts, Rep. AFCRL-TR-75-0185, 1975.

[34] K. Copeland, private communication, 2004.

[35] J. Clem and L. Dorman, "Neutron monitor response functions," *Space Sci. Rev.*, vol. 93, no. 1–2, pp. 335–363, 2000.

[36] A. Belov, A. Struminsky, and V. Yanke, "Neutron monitor response functions for galactic and solar cosmic rays," in *Proc. 1999 ISSI Workshop on Cosmic Rays and Earth*, 1999.

[37] V. Mares, S. Roesler, and H. Schraube, "Averaged particle dose conversion coefficients in air crew dosimetry," *Radiat. Prot. Dosim.*, vol. 110, no. 1–4, pp. 371–376, Sep. 2004.

[38] *Measurement and Reporting of Alpha Particle and Terrestrial Cosmic Ray-Induced Soft Errors in Semiconductor Devices*, JEDEC Standard JESD89, August 2001.